Supporting information

A Liquid-like Quasi-solid Polymer Electrolyte for High-performance Sodium Metal Batteries

Vineeth Sasikumar Kala,[1,2,3] Chhail Bihari Soni,[1] Sungjemmenla,[1] Mahesh Chandra,[1] Sanjaykumar C.,[1] Arihant Bhandari,[1] Yusuke Yamauchi,[3,4,5] Minsu Han,[3,4]* and Vipin Kumar[1,2]*

[1]Department of Energy Science and Engineering, Indian Institute of Technology Delhi, Hauz Khas, New Delhi, India 110016

[2]University of Queensland- IIT Delhi Academy of Research (UQIDAR), Indian Institute of Technology Delhi, Hauz Khas, New Delhi, India 110016

[3]Australian Institute for Bioengineering and Nanotechnology (AIBN), The University of Queensland, Brisbane, QLD 4072, Australia

[4]Department of Materials Process Engineering, Graduate School of Engineering, Nagoya University, Nagoya 464-8603, Japan

[5]Department of Chemical and Biomolecular Engineering, Yonsei University, 50 Yonsei-ro, Seodaemun-gu, Seoul 03722, Republic of Korea

Corresponding author E-mail - vkumar@dese.iitd.ac.in

1. Experimental

1.1. Materials

Poly(vinylidene fluoride-co-hexafluoropropylene) (PVDF-HFP, average Mw 455,000), poly(ethylene glycol)-block-poly(propylene glycol)-block-poly(ethylene glycol) (PEG-PPG-PEG, average Mn 20,000), acetone, dimethyl carbonate (DMC, anhydrous, 99%), and ethylene carbonate (EC, anhydrous, 99%) were purchased from Sigma-Aldrich. Fluoroethylene carbonate (FEC) and sodium perchlorate ($NaClO_4$, ACS reagent, ≥98.0%) were procured from TCI chemicals.

Precursors for the cathode, including Super-P (Thermo Scientific) as the conductive agent, poly(vinylidene fluoride) (PVDF, average Mw ~534,000 by GPC) as the binder, and 1-methyl-2-pyrrolidinone (NMP, anhydrous, 99.5%) as the solvent, were obtained from Sigma-Aldrich. Iron (II) sulfate heptahydrate and sodium ferrocyanide decahydrate were also obtained from Sigma-Aldrich. All the materials were dried overnight at 60 °C in a hot air oven before use.

1.1.1. Preparation of PVDF-HFP/PEG-PPG-PEG blend membranes and their use in QSPE fabrication

A solution blending technique was employed to prepare PVDF-HFP and PEG-PPG-PEG blends in various weight ratios. The polymers were dissolved in acetone at 50 °C, taking care to prevent solvent loss. After complete dissolution, the solution was heated for an additional 3 h to evaporate the acetone until a highly viscous state was reached. The viscous blend solution was then cast onto aluminum foil using a slurry coater at a speed of 5 mm s^{-1}. To ensure complete removal of residual solvent, the cast film was further dried at 60 °C for 3 h. The resulting free-standing membrane was peeled off and cut into discs with a diameter of 18 µm to match the separator dimensions. The membranes were labeled as pristine_100 (PVDF-HFP: PEG-PPG-PEG = 100:0), blend_90-10 (90:10), blend_80-20 (80:20), blend_70-30 (70:30), and blend_60-40 (60:40), according to the weight ratio of PVDF-HFP to PEG-PPG-PEG. QSPEs were prepared by soaking the membranes in 1 M $NaClO_4$ in EC: DMC (1:1 by volume) with FEC additive, inside an argon-filled glove box.

1.1.2. Preparation of cathodes for sodium metal battery applications

A Prussian blue (PB)-based cathode was employed in this study. PB was synthesized using a modified version of previously reported methods [1,2]. The synthesized PB was characterized by X-ray diffraction (XRD) and Fourier-transform infrared spectroscopy (FTIR). The sample was stored at 60 °C to prevent moisture absorption.

The cathode slurry was prepared using a weight ratio of PB powder: Super P: PVDF = 7:2:1. The binder solution was made by dissolving PVDF in NMP at 60 °C for 1 h, followed by the addition of PB and Super P. To ensure homogeneity, the mixture was stirred overnight at 60 °C. The resulting slurry was cast onto carbon-coated aluminum foil using an STC-TMH250 film tape casting machine and dried at 50 °C overnight. The cathode was then punched into 15 mm diameter disks and transferred to an argon-filled glove box (H_2O, O_2< 1 ppm) for further battery assembly.

1.2. Characterization

1.2.1. Structural and physicochemical property analysis

Fourier-transform infrared spectroscopy (FTIR) analysis was performed using a Nicolet iS560 FTIR spectrometer to investigate the structural properties. Spectra were recorded in the range of 3500 to 400 cm^{-1}, with a resolution of 4 cm^{-1}. A background scan was performed before measurement to minimize errors, and all analyses were carried out in reflectance mode. Phase analysis of the blended polymer films was performed using XRD with a Ragaku Ultima IV diffractometer. Samples were pre-dried at 60 °C for 3 h before analysis, and the analysis was conducted at a scan rate of 5° min^{-1}.

Electrolyte uptake (%) was evaluated by soaking the polymer host membranes in excess liquid electrolyte (LE; 1 M $NaClO_4$ in EC-DMC with FEC). The test also assessed the optimal activation time. The electrolyte uptake (%) was calculated using the following equation:

$$Electrolyte\ uptake\ (\%) = \frac{(W_2 - W_1)}{W_1} \times 100$$

where W_2 represents the weight of the wet polymer sample after soaking, and W_1 is the dry weight before soaking.

Porosity was analyzed using the n-butanol adsorption method [3,4]. The dry mass (W_d) and volume (V) of the polymer host were measured, after which the samples were immersed in n-butanol for 1 h. Excess solvent was carefully removed, and the wet weight (W_w) was recorded.

To ensure accuracy, each measurement was repeated three times. ρ represents the density of n-butanol.

Porosity (%) was calculated using the following equation:

$$Porosity\ (\%) = \frac{(W_w - W_d)}{V \cdot \rho} \times 100$$

1.2.2. FESEM and elemental mapping analysis

Field-emission scanning electron microscopy (FESEM) was used to examine the morphology of the polymer host and cycled sodium metal, along with elemental analysis via energy-dispersive X-ray spectroscopy (EDS). FESEM was performed in JEOL JSM-7800F, and EDS analysis was conducted with Zeiss EVO 50 & EVO 18. Gold sputtering was applied to the non-conductive polymer samples before imaging.

1.2.3. Mechanical and thermal analysis

Mechanical properties were assessed via stress-strain measurements using Zwick Roell, Germany static Universal Testing Machine (UTM Z010 (Static)) at a deformation rate of 5 mm min^{-1}, in accordance with ASTM D882 standard. Thermal properties were characterized by thermogravimetric analysis with derivative thermogravimetry (TGA-DTG) and differential scanning calorimetry (DSC). DSC measurements were performed using a DSC2500 under a nitrogen atmosphere (40 mL min^{-1} flow) in the temperature range of 25 to 250 °C, and the area under the DSC curves was analyzed using TRIOS software. The heating rate was set to 20 °C min^{-1}. TGA-DTG analysis was carried out using a Simultaneous Thermal Analyzer (SDT650), under a nitrogen atmosphere at a heating rate of 10 °C min^{-1}, over the range of 25 to 600 °C.

1.2.4. Electrochemical analysis

A 2032-type coin cell symmetric cell was assembled in an argon-filled glove box to evaluate ionic conductivity. The cell consisted of stainless steel (SS) blocking electrodes sandwiching the QSPE, with thickness l (cm) and A (cm^2). The ionic conductivity was measured using electrochemical impedance spectroscopy (EIS) over a frequency range of 0.1 Hz to 100 kHz. To examine the temperature dependence of conductivity, measurements were taken at 25 °C, 30 °C, 35 °C, 40 °C, 45 °C, 50 °C, and 60 °C. From the impedance spectra, the bulk resistance (R_b) was extracted from the high-frequency intercept on the Z'-axis of the Nyquist plot. Ionic conductivity (σ, mS cm^{-1}) was calculated using the equation:

$$\sigma = \frac{l}{R_b \cdot A}$$

Na^+ transference number (t_{Na^+}) was determined by chronoamperometry on Na//QSPE//Na symmetric cells using the Bruce-Vincent method. For comparison, the transference number of the LE was also measured. The transference number was calculated as:

$$t_{Na}{}^{+} = \frac{I_{ss}(\Delta V - I_0 R_0)}{I_0(\Delta V - I_{ss} R_s)}$$

where I_0 is the initial current, I_{ss} is the steady-state current, ΔV is the applied voltage (10 mV), R_0 is the initial interfacial resistance, and R_s is the interfacial resistance after polarization. Impedance spectra were recorded from 0.1 Hz to 100 kHz.

The electrochemical stability window (ESW) of QSPEs was investigated using linear sweep voltammetry (LSV) in Na//QSPE//SS cells over a potential range of -0.5 to 6 V at a scan rate of 10 mV s^{-1}, using a Corrtest CS350 electrochemical workstation. Cyclic plating/stripping performance was analyzed using Na//QSPE//Na symmetric cells under a current density of 1.0 mA cm^{-2} and a capacity of 1.0 mAh cm^{-2}. Tafel analysis was also performed using the same configuration, with LSV conducted from −0.3 V to 0.3 V at a scan rate of 5.0 mV s^{-1}.

For charge-discharge cycling and rate performance evaluations, full cells were constructed with sodium metal as the anode, QSPE as the electrolyte, and PB as the cathode. The voltage window was set from 2.0 to 4.0 V, and the PB cathode had an active material loading of 1.0 mg cm^{-2}. Cells were rested for 4 h before testing and evaluated using a computer-controlled NEWARE BTS 3000 battery tester. For post-mortem analysis, cycled cells were disassembled in the glove box, and electrode morphology was examined via SEM. Cyclic voltammetry (CV) of Na//blend_70-30 QSPE//PB cells was conducted at a scan rate of 0.1 mV s^{-1} within a potential range of 2.0 to 4.0 V *vs.* Na/Na^+.

2. Computational

2.1. Transport properties: diffusion coefficients, ionic conductivity, and transference number

The total ionic conductivity of the complex electrolyte system can be calculated using Onsager transport coefficients [5]. In general, the conductivity is given by:

$$\sigma = e^2 \sum_i \sum_j L^{ij} z_i z_j \quad (1),$$

where e is the elementary charge, $z_{Na^+} = 1$, $z_{ClO_4^-} = -1$, and L^{ij} are the Onsager transport coefficients, which are calculated as:

$$L^{ij} = \frac{N^i N^j}{2dVk_BT} \lim_{t\to\infty} \frac{d}{dt} S^{ij}(t) \quad (2),$$

where N^i and N^j are the number of ions of species i and j, $d = 3$ is the system dimensionality, V is the volume, k_B is the Boltzmann's constant, T is the temperature, and $S^{ij}(t)$ is defined as:

$$S^{ij}(t) = \left\langle \Delta\vec{R}_{CM}^{\,i}(t) \cdot \Delta\vec{R}_{CM}^{\,j}(t) \right\rangle \quad (3).$$

The right-hand side denotes the statistical average of the dot product of the center-of-mass displacements of ions of species i and j over an ensemble of trajectories. The calculated $S^{Na^+\,Na^+}$ and $S^{ClO_4^-\,ClO_4^-}$ are shown in **Figure S10**. After an initial kink, both curves exhibit a linear increase with time.

The Onsager coefficients L^{ij} are extracted from the slope of $S^{ij}(t)$ with time as per Eq. 2. The diffusion coefficient is closely related to the Onsager coefficient [6]:

$$D^i = Vk_BT \frac{L^{ii}}{N^i} \quad (4).$$

The calculated diffusion coefficient is found to be 2.57×10^{-6} cm^2 s^{-1} for Na^+ and 3.41×10^{-7} cm^2 s^{-1} for ClO_4^-. The total conductivity also includes cross-correlation terms, where $i = Na^+$ and $j = ClO_4^-$. By symmetry $S^{ij} = S^{ji}$ and $L^{ij} = L^{ji}$. Hence, the conductivity in Eq. 1 can be simplified for the case of univalent electrolytes as:

$$\sigma = e^2 \left(L^{Na^+\,Na^+} - 2L^{Na^+\,ClO_4^-} + L^{ClO_4^-\,ClO_4^-} \right) \quad (5)$$

The calculated conductivity from Eq. 5 is found to be 2.10 mS cm^{-1}. Further, the transference number can be calculated from Onsager coefficients as:

$$t_i = \frac{\sum_j L^{ij} z_i z_j}{\sum_m \sum_n L^{mn} z_m z_n} \quad (6).$$

From Eq. 6 we compute a transference number of $t_{Na^+} = 0.9$, which is higher than the experimentally measured value of $t_{Na^+} = 0.78$. The computational results depend upon the

chain length of the polymer (see [5]). Conductivity and the transference numbers typically decrease with an increase in the chain length. As the chain length that is considered in the computational simulation is much smaller than in experiments, the computations are an upper bound to the conductivity and transference number achievable in these systems.

3. Results

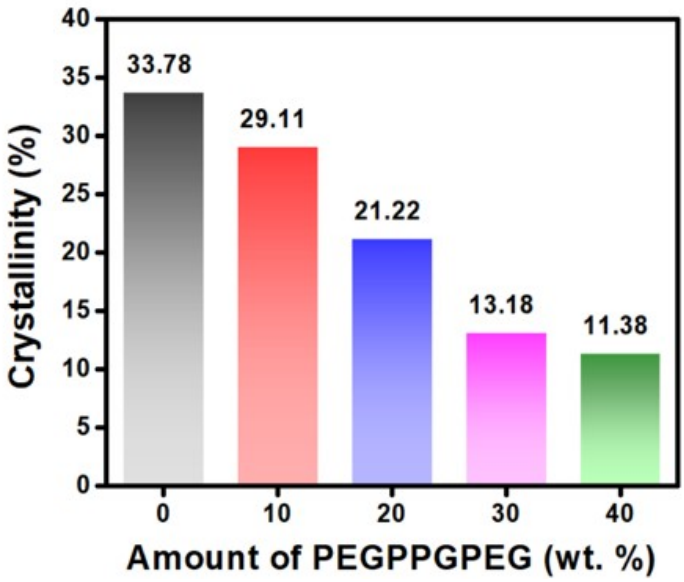

Figure S1. Degree of crystallinity (X_{XRD}, %) of polymer blend membranes calculated from XRD patterns.

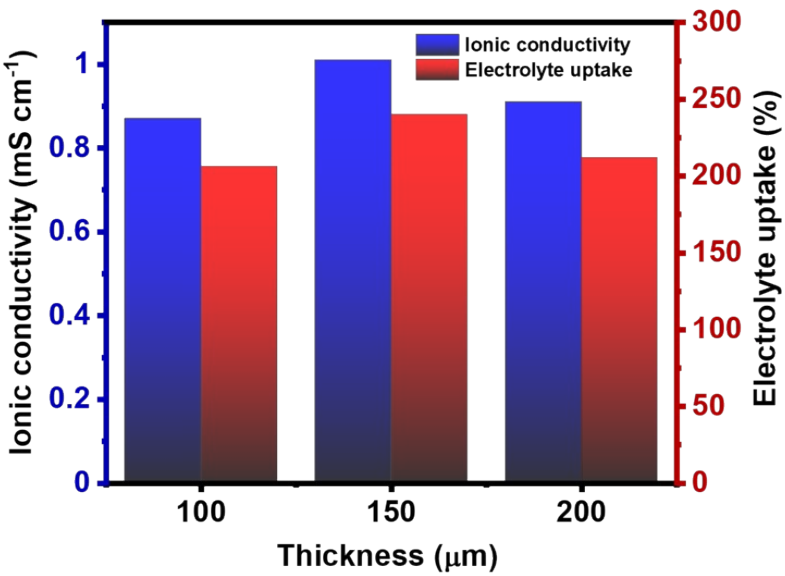

Figure S2. Thickness dependence of room-temperature ionic conductivity and electrolyte uptake in blend_70-30 membranes.

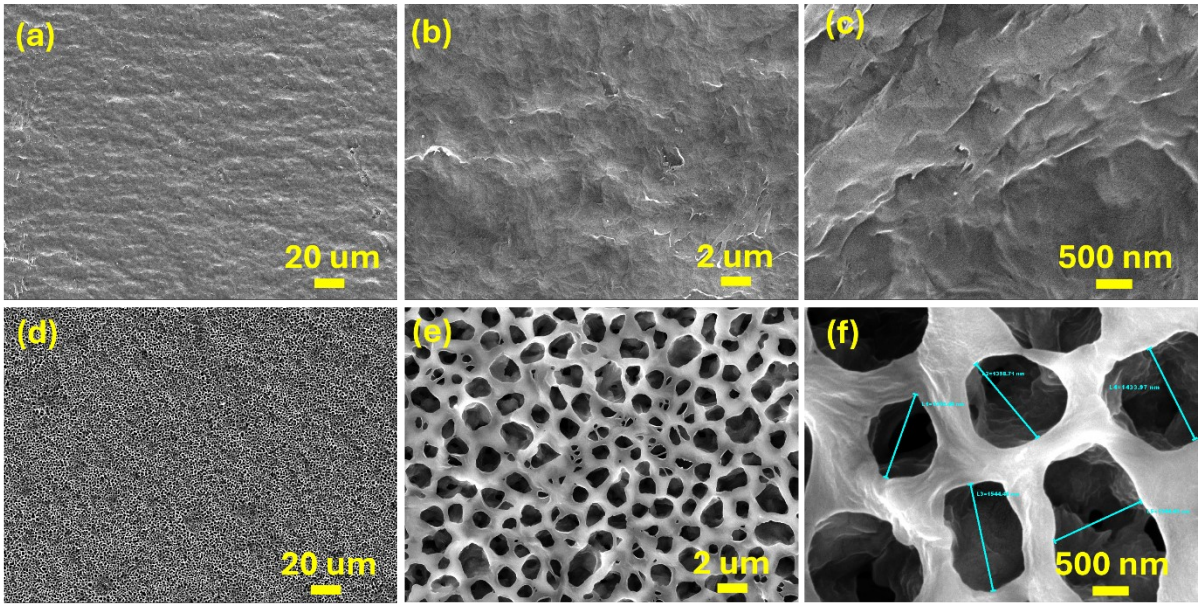

Figure S3. FESEM images at different magnifications for (a-c) pristine_100 and (d-f) blend_70-30 membranes.

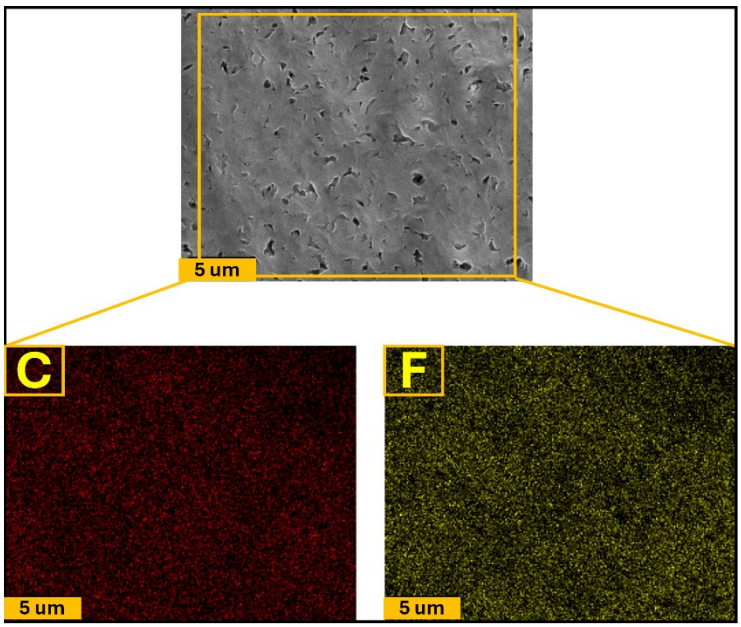

Figure S4. Elemental mapping of pristine_100 observed by FESEM-EDS.

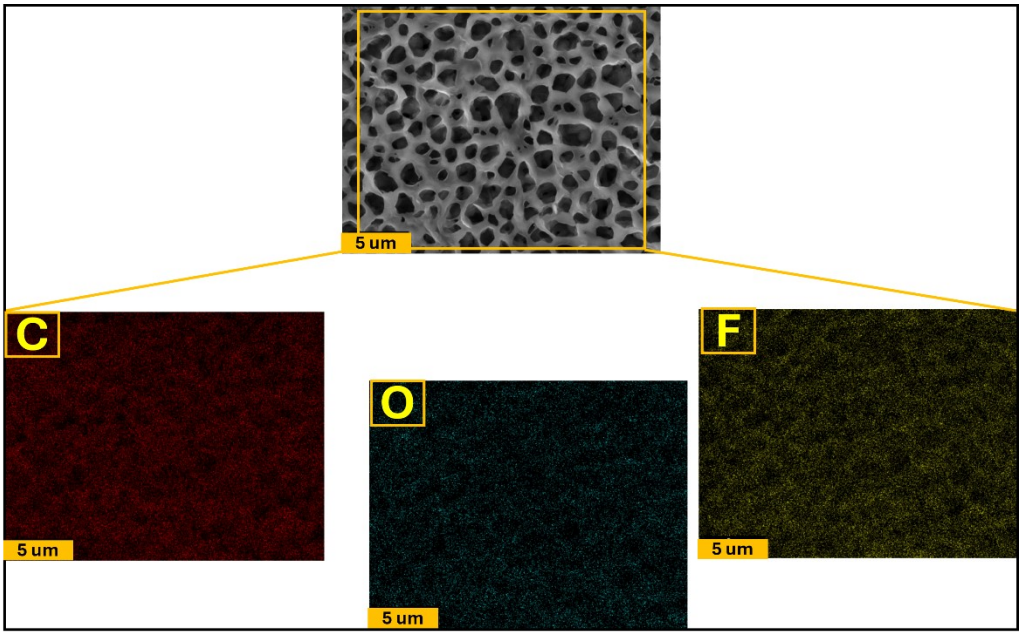

Figure S5. Elemental mapping of blend_70-30 observed by FESEM-EDS.

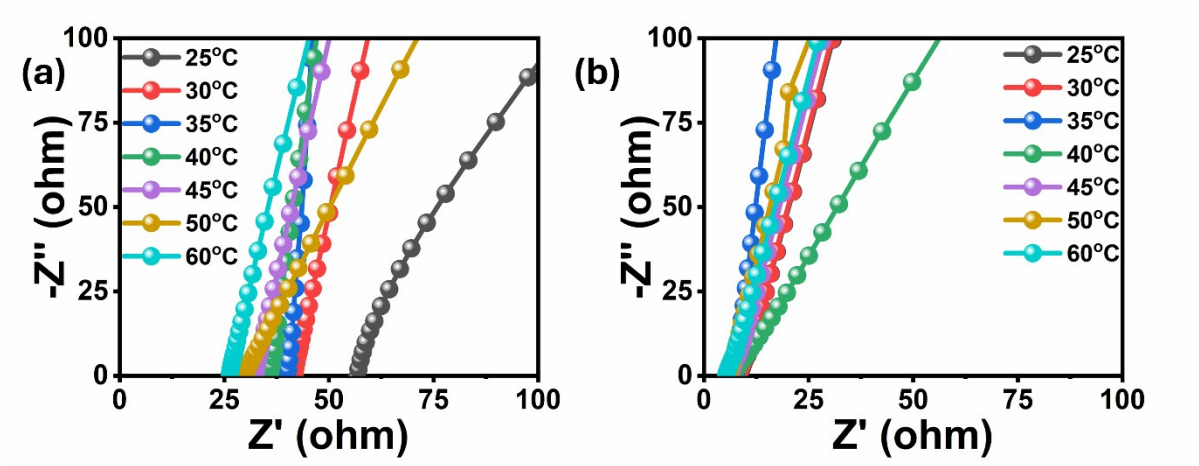

Figure S6. EIS results at various temperatures for (a) pristine_100 and (b) blend_70-30 QSPEs.

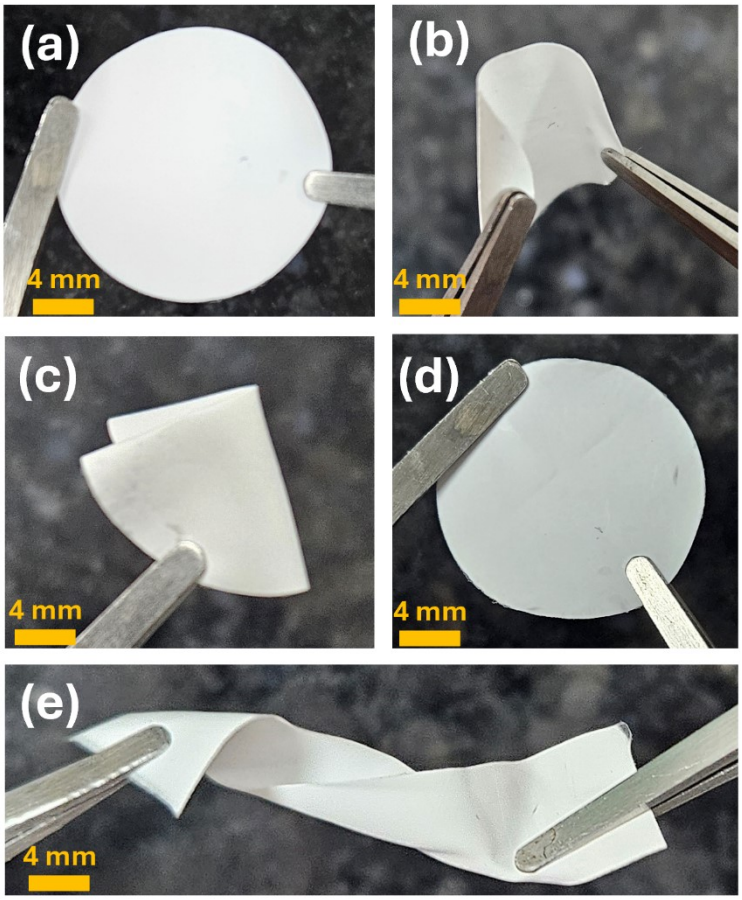

Figure S7. Optical images of blend_70-30 membrane under different mechanical deformations: (a) original, (b) bent, (c) folded, (d) recovered after bending and folding, and (e) twisted.

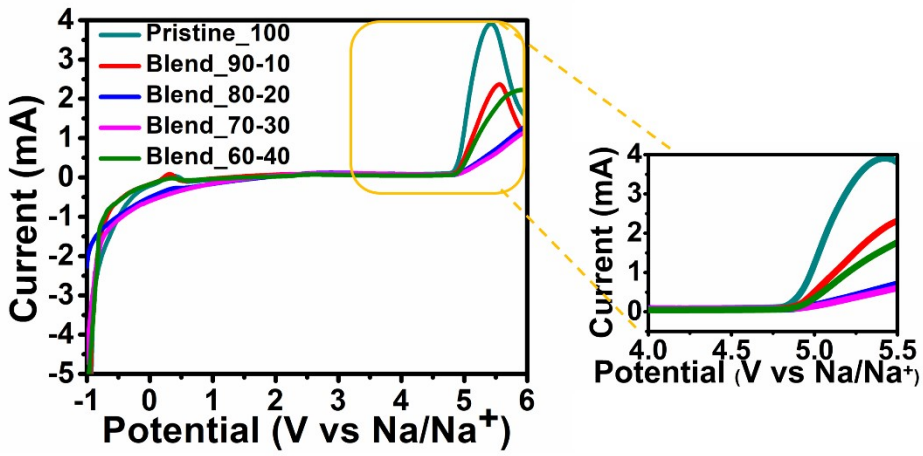

Figure S8. Overlaid ESWs for the QSPEs employed.

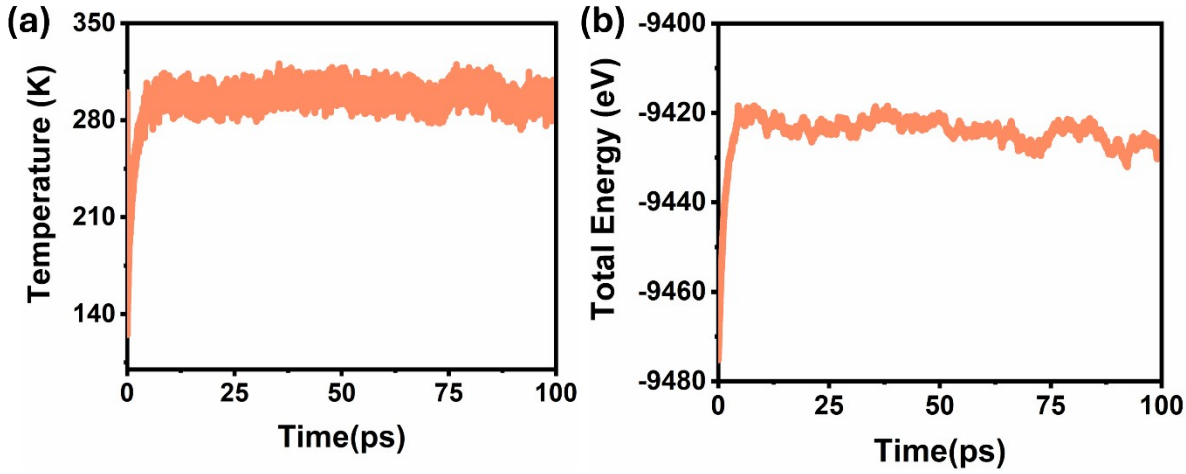

Figure S9. Temperature and total energy profiles during the MD simulation of the blend_70-30 QSPE system.

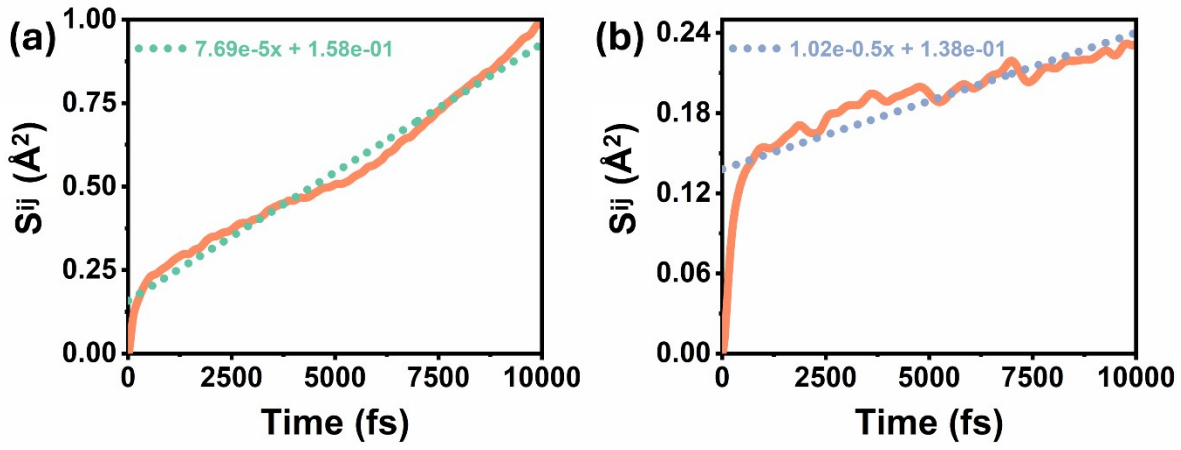

Figure S10. Calculated $S^{ij}(t)$ for (a) $i = j = Na^{+}$ and (b) $i = j = ClO_4^{-}$.

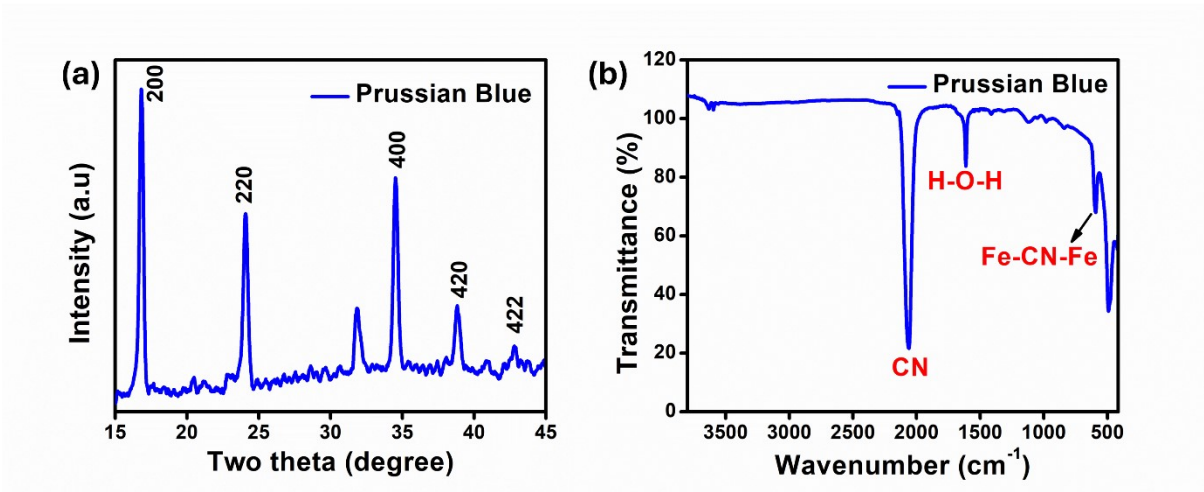

Figure S11. Characterization of the synthesized PB: (a) XRD pattern and (b) FTIR spectrum.

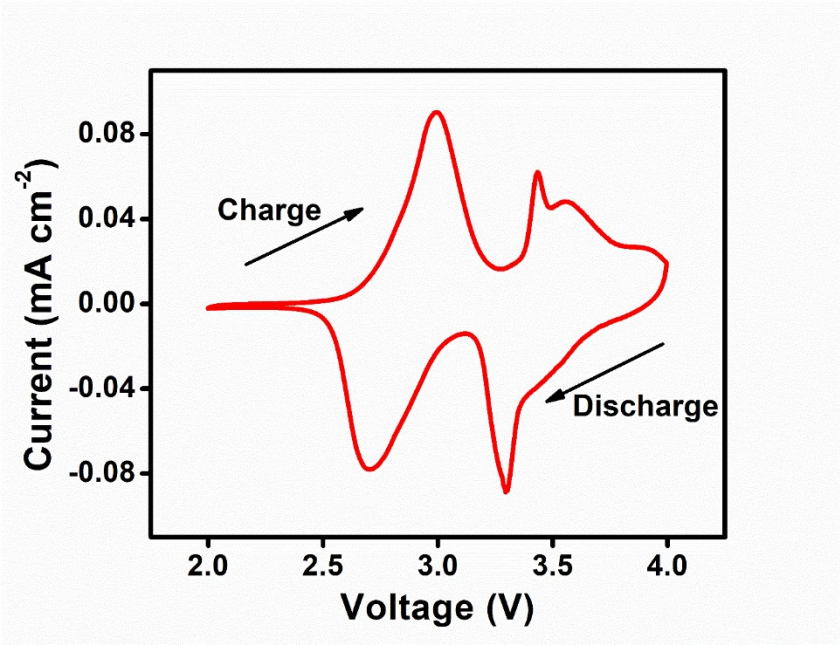

Figure S12. Cyclic voltammetry curve of the PB cathode paired with a Na metal anode and blend_70-30 QSPE, recorded at a scan rate of 0.1 mV s^{-1} within a potential window of 2.0-4.0 V *vs.* Na/Na^{+}.

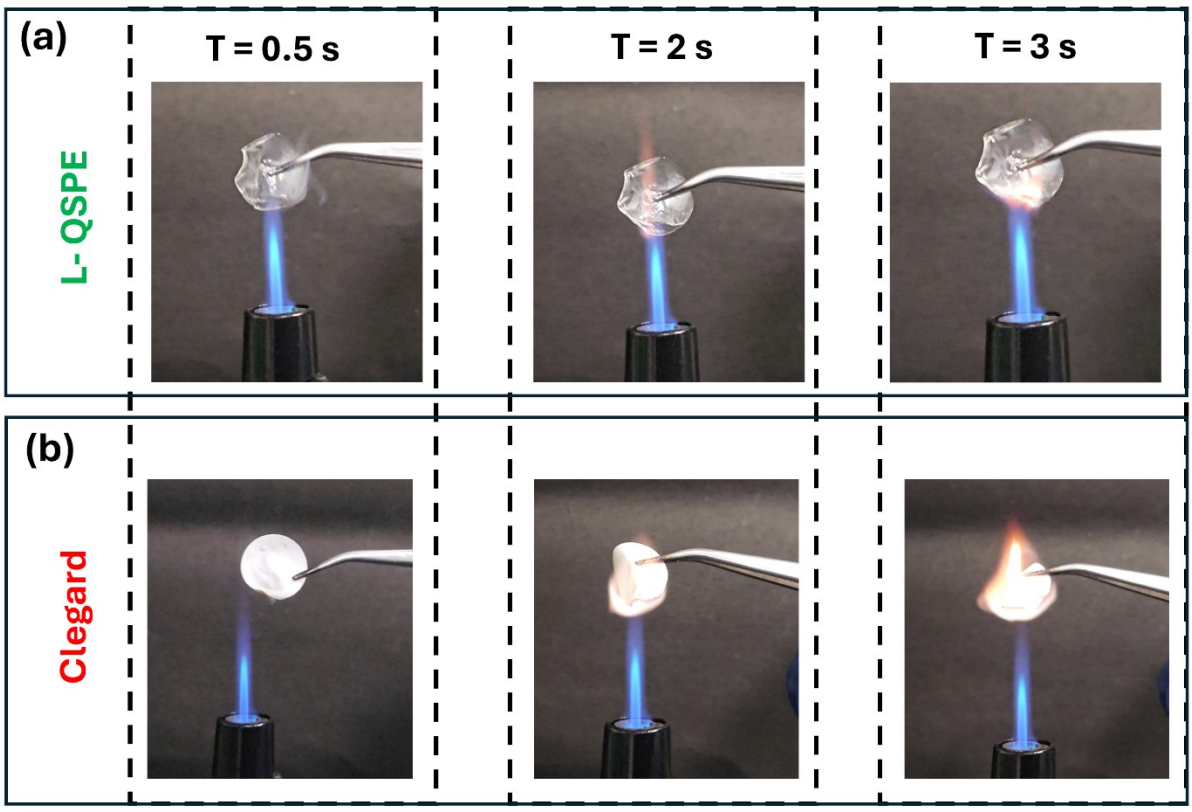

Figure S13. Optical photographs of flame tests conducted at various time intervals for the L-QSPE and a commercial Celgard separator soaked with LE.

Table S1. Comparison of the electrochemical performance of the present L-QSPE system with previously reported QSPEs used in SMBs.

Sl. No.	Electrolyte composition	Ionic conductivity ($S\ cm^{-1}$), Temperature (°C)	Cathode	Cycle number, C rate
1	PVDF-HFP/PEG-PPG-PEG $NaClO_4$-EC/DMC/FEC (**Present work**)	1.01×10^{-3}, 25°C	Prussian blue (PB)	600, 0.5 C
2	PVDF-HFP soaked in sodium–poly(tartaric acid)borate/ PC (1:2, wt. %) [7]	0.94×10^{-4}, 30°C	$Na_3V_2(PO_4)_3$	500, 0.5 C
3	PETEA copolymer-NaTFSI-PC/FEC [8]	3.85×10^{-3}, 25°C	poly(S-PETEA)-based sulfur cathode	100, 0.1 C
4	PVDF-HFP-GO-$NaClO_4$-EC/PC [9]	2.3×10^{-3}, 25°C	$Na_3V_2(PO_4)_3$	1100, 1 C
5	Thermoplastic PU-$NaClO_4$- EC/DEC/FEC [10]	1.5×10^{-3}, 25°C	$Na_3V_2(PO_4)_3$	100, 1 C and 2 C
6	PEO-Cu MOF- $NaClO_4$-EC/DEC/FEC [11]	3.48×10^{-3}, 25°C	$NaCrO_2$	800, 1 C
7	Poly EPTA- $NaPF_6$-PC:EMC:FEC [12]	5.33×10^{-3}, 25°C	Graphite	1000, 100 mA g^{-1}
8	(P(MVE-alt-MA))-bacterial cellulose (BC)-triethyl phosphate-$NaClO_4$-VC[13]	2.2×10^{-4}, 25°C	$Na_3V_2(PO_4)_3$	1000, 1 C
9	PVDF-HFP- β/β″-Al_2O_3- $NaClO_4$-	7.13×10^{-4}, 25°C	$Na_3V_2(PO_4)_3$	1000, 1 C

	EC/DEC/FEC [14]			

4. References

1 Y. Qiao, G. Wei, J. Cui, M. Zhang, X. Cheng, D. He, S. Li and Y. Liu, *Chem. Commun.*, 2019, **55**, 549–552.

2 S. K. Vineeth, C. B. Soni, Sungjemmenla, C. Sanjaykumar, Y. Yamauchi, M. Han and V. Kumar, *J. Energy Storage*, 2023, **73**, 108780.

3 D. Deb, P. Bose and S. Bhattacharya, *Ionics (Kiel).*, 2021, **27**, 123–136.

4 W. Ren, Y. Huang, X. Xu, B. Liu, S. Li, C. Luo, X. Li, M. Wang and H. Cao, *J. Mater. Sci.*, 2020, **55**, 12249–12263.

5 K. D. Fong, J. Self, B. D. McCloskey and K. A. Persson, *Macromolecules*, 2020, **53**, 9503–9512.

6 N. M. Vargas-Barbosa and B. Roling, *ChemElectroChem*, 2020, **7**, 367–385.

7 L. Yang, Y. Jiang, X. Liang, Y. Lei, T. Yuan, H. Lu, Z. Liu, Y. Cao and J. Feng, *ACS Appl. Energy Mater.*, 2020, **3**, 10053–10060.

8 D. Zhou, Y. Chen, B. Li, H. Fan, F. Cheng, D. Shanmukaraj, T. Rojo, M. Armand and G. Wang, *Angew. Chemie Int. Ed.*, 2018, **57**, 10168–10172.

9 C. Luo, T. Shen, H. Ji, D. Huang, J. Liu, B. Ke, Y. Wu, Y. Chen and C. Yan, *Small*, 2020, **16**, 1906208.

10 M. Park, H. Woo, J. Heo, J. Kim, R. Thangavel, Y. Lee and D. Kim, *ChemSusChem*, 2019, **12**, 4645–4654.

11 Z. Zhang, Y. Huang, C. Li and X. Li, *ACS Appl. Mater. Interfaces*, 2021, **13**, 37262–37272.

12 X. Xu, K. Lin, D. Zhou, Q. Liu, X. Qin, S. Wang, S. He, F. Kang, B. Li and G. Wang, *Chem*, 2020, **6**, 902–918.

13 J. Yang, M. Zhang, Z. Chen, X. Du, S. Huang, B. Tang, T. Dong, H. Wu, Z. Yu, J. Zhang and G. Cui, *Nano Res.*, 2019, **12**, 2230–2237.

14 D. Lei, Y. B. He, H. Huang, Y. Yuan, G. Zhong, Q. Zhao, X. Hao, D. Zhang, C. Lai, S. Zhang, J. Ma, Y. Wei, Q. Yu, W. Lv, Y. Yu, B. Li, Q. H. Yang, Y. Yang, J. Lu and F.

Kang, *Nat. Commun.*, 2019, **10**, 1–11.